The Astrophysical Journal Letters, 710:L49–L52, 2010 February 10 doi:10.1088/2041-8205/710/1/L49

NITROGEN ISOTOPIC FRACTIONATION IN INTERSTELLAR AMMONIA

D. C. Lis[1], A. Wootten[2], M. Gerin[3], and E. Roueff[4]
[1] California Institute of Technology, Cahill Center for Astronomy and Astrophysics 301-17, Pasadena, CA 91125, USA; dcl@caltech.edu
[2] National Radio Astronomy Observatory, 520 Edgemont Road, Charlottesville, VA 22903, USA; awootten@nrao.edu
[3] LERMA, CNRS UMR8112, Observatoire de Paris and École Normale Supérieure, 24 Rue Lhomond, 75231 Paris Cedex 05, France; maryvonne.gerin@lra.ens.fr
[4] LUTh, CNRS UMR8102, Observatoire de Paris, Section de Meudon, Place J. Janssen, 92195 Meudon, France; evelyne.roueff@obspm.fr
Received 2009 November 6; accepted 2009 December 30; published 2010 January 20

ABSTRACT

Using the Green Bank Telescope, we have obtained accurate measurements of the $^{14}N/^{15}N$ isotopic ratio in ammonia in two nearby cold, dense molecular clouds, Barnard 1 and NGC 1333. The $^{14}N/^{15}N$ ratio in Barnard 1, 334 ± 50 (3σ), is particularly well constrained and falls in between the local interstellar medium/proto-solar value of ~450 and the terrestrial atmospheric value of 272. The NGC 1333 measurement is consistent with the Barnard 1 result, but has a larger uncertainty. We do not see evidence for the very high ^{15}N enhancements seen in cometary CN. Sensitive observations of a larger, carefully selected sample of prestellar cores with varying temperatures and gas densities can significantly improve our understanding of the nitrogen fractionation in the local interstellar medium and its relation to the isotopic ratios measured in various solar system reservoirs.

Key words: astrochemistry – ISM: abundances – ISM: individual objects (Barnard 1, NGC 1333) – ISM: molecules – molecular processes – radio lines: ISM

1. INTRODUCTION

Molecular isotopic ratios are an important tool in the study of the origin of interstellar and solar system materials. After hydrogen, nitrogen displays the largest isotopic variations in the solar system, typically explained by mixing of various proto-solar or pre-solar reservoirs. Earth, Mars interior, Venus, and most primitive meteorites have nitrogen isotopic ratios within 5% of the terrestrial atmospheric value, $^{14}N/^{15}N = 272$ (see Marty et al. 2009). However, the proto-solar nebula was poorer in ^{15}N, with $^{14}N/^{15}N \simeq 450$, as evidenced by infrared and in situ measurements in the Jupiter atmosphere (530^{+380}_{-170}, ISO, Fouchet et al. 2000; 435 ± 57, Galileo, Owen et al. 2001; 448 ± 62, Cassini, Abbas et al. 2004; 450 ± 106, Cassini, Fouchet et al. 2004) and recent solar wind measurements (442 ± 131, 2σ, Genesis, Marty et al. 2009). The proto-solar $^{14}N/^{15}N$ ratio is in agreement with the local interstellar medium (ISM) value (450 ± 22, Wilson & Rood 1994; or 414 ± 32 at the birth place of the Sun, Wielen & Wilson 1997).

Very low nitrogen isotopic ratios, $^{14}N/^{15}N = 148 \pm 6$, have been measured in CN in a large sample of comets (Manfroid et al. 2009). Similar isotopic ratios have been recently derived by Bockelée-Morvan et al. (2008) in comet 17P/Holmes in CN and HCN, the presumed parent of the CN radical in cometary atmospheres ($^{14}N/^{15}N = 165 \pm 40$ and 139 ± 26, respectively). Although higher ratios in HCN were initially reported in comet Hale-Bopp, Bockelée-Morvan's re-analysis of the archival data suggests that the $^{14}N/^{15}N$ ratio in HCN in this comet is also consistent with the CN value, given the measurement uncertainties. The exact chemical networks explaining the HCN isotopic anomaly in comets have yet to be proposed. However, one clear conclusion is that HCN has never isotopically equilibrated with the nebular N_2 at the later phases of the evolution of the solar system (Bockelée-Morvan et al. 2008). Low nitrogen isotopic ratios are also found in some meteorites, interplanetary dust particles (IDPs), and samples of material returned from comet 81P/Wild 2 by the Stardust spacecraft; amine groups in particular often show low $^{14}N/^{15}N$ ratios (Engel & Macko 1997; Keller et al. 2004; Floss et al. 2006; McKeegan et al. 2006).

In the ISM, nitrogen bearing molecules are important tracers of cold, dense gas, as they do not freeze out onto grain mantles at densities below a few $\times 10^6$ cm^{-3}, in contrast to carbon and oxygen species, such as CO or CS. In cold, dense, CO depleted ISM regions, high ^{15}N enhancements have been suggested to be present in gas-phase molecules, in particular in ammonia (see Rodgers & Charnley 2008a, 2008b, and references therein). These isotopic enhancements could be preserved as spatial heterogeneity in ammonia ice mantles, as monolayers deposited at different times would have different isotopic compositions and may in turn explain the ^{15}N enhancements seen in primitive solar system refractory organics, if they are synthesized from ammonia.

Measurements of nitrogen isotopic ratios in ammonia in cold molecular clouds are of great interest, as they provide quantitative observational constraints for the chemical fractionation models. However, the data available are scarce. In a recent study, Gerin et al. (2009) detected a doubly fractionated ammonia isotopologue, $^{15}NH_2D$, in several ISM regions. They derive $^{14}N/^{15}N$ isotopic ratios ~350–850, similar to the proto-solar value of 450. However, the $^{15}NH_2D$ lines are weak, and the corresponding measurement uncertainties are large. To better constrain the nitrogen isotopic ratios in the solar neighborhood, we have observed the $^{14}NH_3$ and $^{15}NH_3$ inversion lines using the NRAO 100 m Robert C. Byrd Green Bank Telescope (GBT). We present here results for two nearby clouds, Barnard 1 and NGC 1333, and discuss prospects for future studies of nitrogen isotopic ratios using the GBT.

2. OBSERVATIONS

Observations of ammonia inversion lines presented here were carried out in 2009 February using the GBT. Conditions were calm under a lightly overcast sky resulting in a stable system temperature of ~48–50 K. The *K*-band receiver feed/amplifier set covering 22–26.5 GHz was employed. The GBT spectrom-

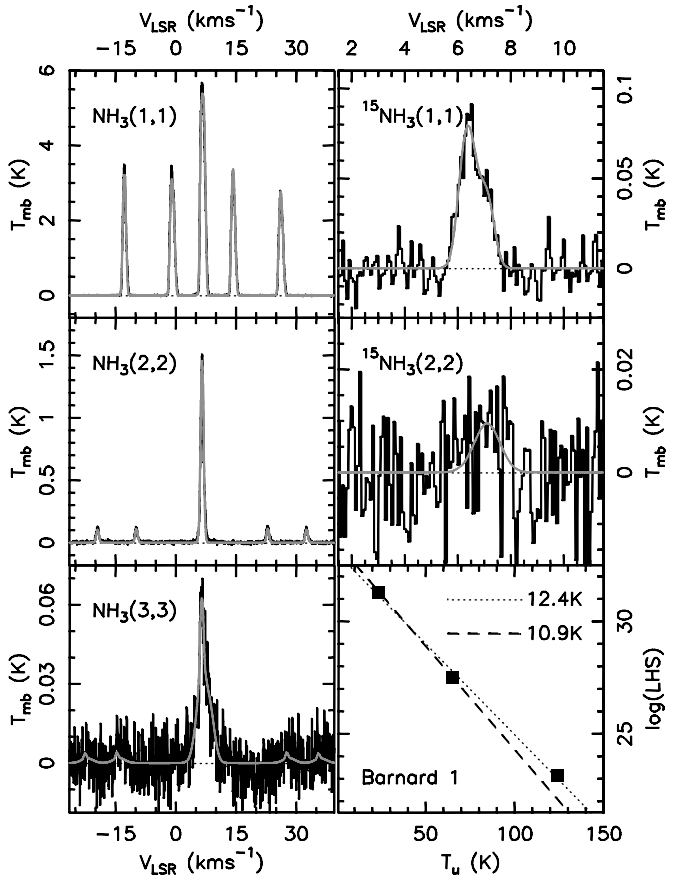

Figure 1. Spectra of the ammonia inversion lines in Barnard 1-b (α_{J2000} = 03^{h}33^{m}20^s.8, δ_{J2000} = +31°07′34″). Gray lines show hyperfine structure fits—a single velocity component for the $^{14}NH_3$(1,1), (2,2), and $^{15}NH_3$ (1,1) transitions and two components for the $^{14}NH_3$ (3,3) transition, as described in the text. The $^{15}NH_3$ (2,2) spectrum, shown with a Gaussian line fit, is formally a 3.5σ upper limits. The bottom-right panels show the local thermodynamic equilibrium (LTE) rotation diagram, as described in the text. LHS stands for the left-hand side in Equation (2) of Blake et al. (1987).

eter was configured in its eight 50 MHz intermediate frequency (IF) bandwidth, nine-level mode, which allows simultaneous coverage of four 50 MHz frequency bands in two polarizations, through the use of offset oscillators in the IF. This mode gives 3.051 kHz channel separation. The IF no. 0 was centered between the (1,1) and (2,2) lines of $^{14}NH_3$, the (3,3) line was centered in IF no. 1 and the (2,1) line in IF no. 3; IF no. 2 was tuned midway between the (1,1) and (2,2) lines of $^{15}NH_3$.

The antenna temperature calibration was achieved by injecting a calibrated, broadband signal from a noise diode. The data were placed on the T_A^* scale (Ulich & Haas 1976) by multiplying by a factor of $e^{\tau A}/\eta_l$, where τ is the zenith opacity (∼0.065 at 23.5 GHz and 0.075 at 22.5 GHz, from an atmospheric model), A is the air mass of the observations, and η_l is the rear spillover efficiency (∼0.99 for the unblocked GBT aperture). The source 0336+3218 was used for pointing and absolute calibration at the beginning of the observation set. The absolute calibration accuracy is conservatively estimated at 20%. Relative accuracy among lines in spectral bandpasses measured at the same time is much better, typically dominated by the random noise of the spectra. The conventional beam efficiency of the GBT at 20 GHz is $\eta_{mb} \simeq 0.79$ and the FWHM beam size is ∼33″. Data were taken in the frequency switching mode, with a frequency displacement of 6 MHz.

Table 1
HFS Fit Results and Ammonia Column Densities

Transition	$T_R^* dv$[a] (K km s^{-1})	V_{LSR} (km s^{-1})	ΔV (km s^{-1})	τ	N_{mol} (cm^{-2})
		Barnard 1-b			
$^{14}NH_3$ (1,1)	37.7 ± 0.006	6.7	0.80	4.0	2.8×10^{15}
$^{14}NH_3$ (2,2)	1.90 ± 0.005	6.5	0.80	0.3	2.8×10^{15}
$^{14}NH_3$ (3,3)	0.076 ± 0.029	6.5	0.80[b]	...	8.0×10^{15}
	0.26 ± 0.11	7.1	3.5	...	...
$^{14}NH_3$ (2,1)	0.012 ± 0.004	...	...	...	...
$^{15}NH_3$ (1,1)[c]	0.106 ± 0.004	6.6	0.63	...	8.4×10^{12}
$^{15}NH_3$ (2,2)	0.013 ± 0.004	...	...	...	...
		NGC 1333			
$^{14}NH_3$ (1,1)	16.4 ± 0.015	7.5	1.2	1.2	8.9×10^{14}
$^{14}NH_3$ (2,2)	2.22 ± 0.07	7.3	1.3	1.1	9.9×10^{14}
$^{14}NH_3$ (3,3)	0.37 ± 0.06	6.8	1.3[b]	...	2.6×10^{15}
	0.61 ± 0.04	4.7	9.5	...	...
$^{14}NH_3$ (2,1)	0.023 ± 0.007	...	...	...	...
$^{15}NH_3$ (1,1)[c]	0.045 ± 0.007	7.2	0.85	...	2.6×10^{12}
$^{15}NH_3$ (2,2)	0.012 ± 0.008	...	...	...	...

Notes. Upper limit for the $^{14}NH_3$ (2,1) and $^{15}NH_3$ (2,2) transitions included for completeness. Molecular column densities are computed assuming LTE with temperatures of 10.9 and 14.7 K for Barnard 1 and NGC 1333, respectively, as described in the text.

[a] Uncertainties are from the HFS fit for the $^{14}NH_3$ (1,1)–(3,3) lines and computed from the rms in the spectra for the remaining weak lines and upper limits.

[b] Fixed parameter.

[c] The hyperfine structure of $^{15}NH_3$ has been recently revised by Bethlem et al. (2008) who give the level energies with unprecedented accuracy. We have calculated the corresponding transition strengths using the theory of Kukolich (1967) and assuming half-integer values of the quantum numbers of the levels involved.

Automatically updated dynamic pointing and focusing corrections were employed based on real-time temperature measurements and a thermal model of the GBT; zero points were adjusted typically every 2 hr or less, using 0336+3218 as a calibrator. The two polarization outputs from the spectrometer were averaged in the final data reduction process to improve the signal-to-noise ratio. The total integration times for Barnard 1 and NGC 1333 are 174 min and 48 min, respectively.

3. RESULTS

Figure 1 shows spectra of the $^{14}NH_3$ and $^{15}NH_3$ inversion lines toward Barnard 1. The satellite hyperfine lines are detected with high signal-to-noise ratios for the (1,1) and (2,2) transitions of $^{14}NH_3$. Results of hyperfine structure (HFS) fits, obtained using the IRAM CLASS software package, are shown in Table 1. The (1,1) and (2,2) $^{14}NH_3$ lines have the same line width of 0.80 km s^{-1}, while the (3,3) spectrum is much broader, indicating the presence of a high-velocity component originating in warmer gas. Consequently, we fitted the (3,3) line with two velocity components, fixing the line width of the first component at the value obtained for the (1,1) and (2,2) lines. All parameters for the second component were allowed to vary in the fit. The $^{15}NH_3$(1,1) line is slightly narrower than the $^{14}NH_3$ (1,1) and (2,2) lines, as expected for an optically thin line. Figure 2 shows the NGC 1333 spectra. The lines are weaker and broader than in Barnard 1. The (3,3) transition shows strong blueshifted emission from the molecular outflow driven by IRAS 4A. The line width derived from the HFS fit to the $^{15}NH_3$ data is significantly smaller than the values obtained for $^{14}NH_3$.

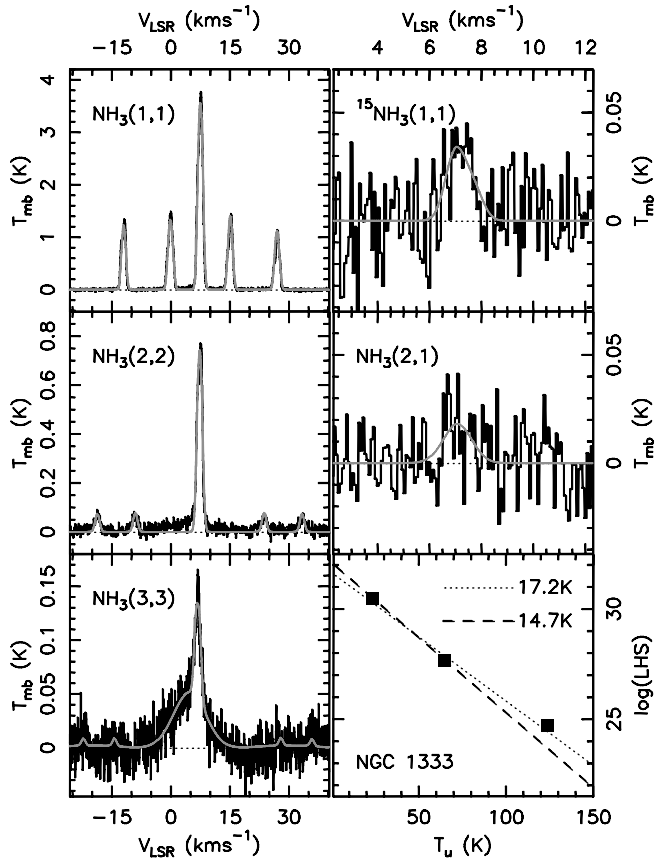

Figure 2. Spectra of the ammonia inversion lines in NGC 1333 (α_{J2000} = $03^{h}29^{m}11\overset{s}{.}6$, δ_{J2000} = +31°13′26″). The $^{14}NH_3$ (2,1) spectrum is formally a 3.7σ upper limit. The bottom-right panel shows the LTE rotation diagram, as described in the text. Lines as in Figure 1.

However, the signal-to-noise ratio in the $^{15}NH_3$ spectrum is relatively low, formally 6.2σ.

We use the rotation diagram technique (see, e.g., Equation (2) of Blake et al. 1987) to derive the excitation temperatures and molecular column densities. We use the spectroscopic constants and partition functions for $^{14}NH_3$ and $^{15}NH_3$ from the JPL Molecular Spectroscopy database (http://spec.jpl.nasa.gov/). The resulting rotation diagrams are shown in Figures 1 and 2, bottom-right panels. The least-squares fit to the line intensities of the (1,1)–(3,3) data (narrow component) in Barnard 1 gives a rotation temperature of 12.4 K in (dotted line in Figure 1). However, since the (3,3) spectrum is contaminated by the high-velocity emission, only the (1,1) transition is detected for $^{15}NH_3$, and given our interest in the cold gas component on the line of sight, a more consistent approach is to use only the (1,1) and (2,2) $^{14}NH_3$ data for the temperature determination. This approach also mitigates possible effects of the non-LTE ortho-to-para ratio (e.g., Umemoto et al. 1999) and results in a slightly lower rotation temperature of 10.9 ± 0.2 K (assuming 2.7% uncertainties for the integrated line intensities, as discussed in Section 4; dashed line in Figure 1, bottom-right panel). This value is subsequently used to derive the $^{14}NH_3$ and $^{15}NH_3$ column densities from the (1,1) integrated line intensities (Table 1). Given the low rotation temperature, we include the correction for the 2.7 K cosmic background radiation in the column density computations. This correction has no effect on the temperature determination, since all the lines observed have very close rest frequencies. The NH_3 temperature and column density in Barnard 1 we derive here are in good agreement with the results of Bachiller et al. (1990) based on observations with the Effelsberg telescope (12 K and 2.5 × 10^{15} cm^{-2}).

For NGC 1333, we derive a rotational temperature of 17.6 K using the (1,1)–(3,3) lines and 14.7 ± 0.5 K using only the (1,1) and (2,2) transitions (dotted and dashed lines, respectively in Figure 2, bottom-right panel). We use the latter value for the column density determination.

4. DISCUSSION

The uncertainty of the derived column densities is difficult to estimate quantitatively. As discussed in Section 2, all lines are observed simultaneously, and the relative calibration is largely determined by the signal-to-noise ratio in the spectra—24 and 6.2σ for $^{15}NH_3$(1,1) in Barnard 1 and NGC 1333, respectively. The $^{14}NH_3/^{15}NH_3$ column density ratio, when computed from the observed intensities of the (1,1) transitions of the two isotopologues, is insensitive to the exact value of the rotation temperature used in the calculations, as long as the temperature is the same for the two isotopologues. The remaining source of uncertainty is the determination of the $^{14}NH_3$ optical depth. The formal uncertainties for the opacity-corrected line intensities given by the HFS fits are negligible (see Table 1). In order to independently estimate the uncertainty of the $^{14}NH_3$ (1,1) integrated line intensities obtained from the HFS fit, we divide the full Barnard 1 data set into three subsets, 58 min integration time each, and fit each subset independently. From the three measurements, we derive a 2.7% uncertainty for the mean which we use as an estimate of the uncertainty of our final $^{14}NH_3$ (1,1) measurement. Adding in quadrature the corresponding statistical uncertainty for $^{15}NH_3$ of 4.2%, we derive a 3σ uncertainty for the $^{14}NH_3/^{15}NH_3$ ratio of 15.0% in Barnard 1. Assuming a 5.2% uncertainty for the $^{14}NH_3$ (1,1) measurement in the shorter NGC 1333 integration (the Barnard 1 value scaled by the square root of the integration time ratio), and adding in quadrature a 16% uncertainty for the $^{15}NH_3$ measurement, we derive a 50% uncertainty (3σ) of the $^{14}NH_3/^{15}NH_3$ ratio in this source. Our final estimates of the $^{14}NH_3/^{15}NH_3$ abundance ratio are thus 334 ± 50 and 344 ± 173 (3σ) for Barnard 1 and NGC 1333, respectively.

The $^{14}N/^{15}N$ fractionation ratios in Barnard 1 and NGC 1333 derived from deuterated ammonia measurements by Gerin et al. (2009) are 470^{+170}_{-100} and 360^{+260}_{-110}, respectively. The NH_3 and NH_2D results are thus consistent, given the NH_2D measurement uncertainties. Owing to the relatively short integration and low SNR in the $^{15}NH_3$ spectrum, our result for NGC 1333 is not very constraining. However, our Barnard 1 data are of excellent quality. The derived $^{14}N/^{15}N$ ratio falls in between the local ISM/proto-solar value (∼450, as discussed in Section 1) and the terrestrial atmospheric ratio of 272. We do not see evidence for the very high ^{15}N enhancements, as suggested by the cometary CN measurements (∼150).

A comparison of our fractionation measurements with the nitrogen "superfractionation" models of Rodgers & Charnley (2008b) is of interest. In their Figure 3, Rodgers & Charnley (2008b) present results of time-dependent models of the evolution of the $^{14}N/^{15}N$ enhancement ratios in key species, including ammonia. For a temperature of 10 K, the gas-phase ^{15}N fractionation in ammonia can reach a maximum enhancement of a factor ∼7–10, much higher than the value we derive for Barnard 1. However, the enhancement factor decreases with time to a factor of a few *below* the initial isotopic ratio assumed in the model. The time at which the maximum fractionation is reached depends strongly on the initial fraction of nitrogen in a molec-

ular form, but is typically of order 1 Myr. The enhancements of the magnitude that we measure can be present very early on, or a few tenths of a Myr after the peak enhancement time.

The Rodgers & Charnley (2008b) model results depend strongly on the gas temperature—significantly higher enhancements are found in the gas-phase ammonia fractionation at 7 K, as compared to 10 K. The sources we have studied are somewhat warmer than the model clouds considered by Rodgers & Charnley (2008b). It would thus be extremely interesting to extend our measurements to colder clouds, such as LDN 1544 or LDN 134N, with central temperatures of order 7 K. Our present observations are exploratory in nature, but show that accurate measurements of nitrogen fractionation in ammonia in cold ISM sources are clearly feasible using the GBT. A focused observing program of a larger, carefully selected sample of prestellar cores with varying temperatures and gas densities would allow significant progress in our understanding of nitrogen fractionation in local ISM and its possible implications for the existing measurements in various solar system reservoirs. Observations of the ground state rotational transitions of ammonia isotopologues using the HIFI instrument aboard the Herschel Space Observatory offer another avenue for measuring ammonia isotopic ratios in dense gas.

The nitrogen fractionation enhancement levels derived here are well reproduced by the gas-phase models of Roueff et al. (see, e.g., Figure 2 of Gerin et al. 2009). For an H_2 density of 10^5 cm^{-3} and a 10 K temperature, the gas-phase models predict $^{14}NH_3/^{15}NH_3 = 389$ and $^{14}NH_2D/^{15}NH_2D = 372$. The models of Roueff et al. are steady-state models that focus on the gas-phase processes and approximate the adsorption of the species on grain surfaces by reducing the elemental abundances in the gas, as compared to the dynamical models of Rodgers & Charnley that explicitly take into account the mantle formation and gas–grain interactions.

We thank T. Minter and the GBT operator, D. Stricklin, for their assistance during the observations and J. Braatz for his advice in setting up the observing scripts. The National Radio Astronomy Observatory is a facility of the National Science Foundation operated under cooperative agreement by Associated Universities, Inc. D. C. Lis is supported by the National Science Foundation grant AST-0540882 to the Caltech Submillimeter Observatory. M. Gerin and E. Roueff acknowledge support from the CNRS-INSU French National Program PCMI (Physique et Chimie du Milieu Interstellaire).

REFERENCES

Abbas, M. M., et al. 2004, ApJ, 602, 1063
Bachiller, R., Menten, K. M., & del Río-Alvarez, S. 1990, A&A, 236, 461
Bethlem, H. L., Kajita, M., Sartakov, B., Meijer, G., & Ubachs, W. 2008, Eur. Phys. J. Spec. Top., 163, 55
Blake, G. A., Sutton, E. C., Masson, C. R., & Phillips, T. G. 1987, ApJ, 315, 621
Bockelée-Morvan, D., et al. 2008, ApJ, 679, L49
Engel, M. H., & Macko, S. A. 1997, Nature, 389, 265
Floss, C., et al. 2006, Geochim. Cosmochim. Acta, 70, 2371
Fouchet, T., et al. 2000, Icarus, 143, 223
Fouchet, T., et al. 2004, Icarus, 172, 50
Gerin, M., et al. 2009, A&A, 498, L9
Keller, L. P., et al. 2004, Geochim. Cosmochim. Acta, 68, 2577
Kukolich, S. G. 1967, Phys. Rev., 156, 83
Manfroid, J., et al. 2009, A&A, 503, 613
Marty, B., et al. 2009, Geochim. Cosmochim. Acta, 74, 340
McKeegan, K. D., et al. 2006, Science, 314, 1724
Owen, T., Mahaffy, P. R., Niemann, H. B., Atreya, S., & Wong, M. 2001, ApJ, 553, L77
Rodgers, S. D., & Charnley, S. B. 2008a, ApJ, 689, 1448
Rodgers, S. D., & Charnley, S. B. 2008b, MNRAS, 385, L48
Ulich, B. L., & Haas, R. W. 1976, ApJ, 30, 247
Umemoto, T., Mikami, H., Yamamoto, S., & Hirano, N. 1999, ApJ, 525, L105
Wielen, R., & Wilson, T. L. 1997, A&A, 326, 139
Wilson, T. L., & Rood, R. T. 1994, ARA&A, 32, 191